nature methods

Brief Communication

https://doi.org/10.1038/s41592-023-02030-7

Molecular mechanocytometry using tension-activated cell tagging

In the format provided by the authors and unedited

Table S1. Representative list of methods for mechanophenotyping.
The majority of past reports describing approaches for mechanical phenotyping use deformability as a marker. Cell deformation is induced by a variety of methods, including narrow constrictions, laser traps, shear stress, and acoustic waves, etc. The table below lists representative papers using deformability as well as adhesion strength or traction forces-based mechanophenotyping methods. Note that all past methods are based on cell-response rather than molecular tension generated by specific adhesion receptors.

Marker	Article Title	Year	Journal
Deformability	Optical Deformability as an Inherent Cell Marker for Testing Malignant Transformation and Metastatic Competence[1]	2005	*Biophysical Journal*
	Analyzing cell mechanics in hematologic diseases with microfluidic biophysical flow cytometry[2]	2008	*Lab on a chip*
	Microfluidics-Based Assessment of Cell Deformability[3]	2012	*Anal. Chem.*
	Microfluidic micropipette aspiration for measuring the deformability of single cells[4]	2012	*Lab on a chip*
	Characterizing deformability and surface friction of cancer cells[5]	2013	*PNAS*
	Pinched-flow hydrodynamic stretching of single-cells[6]	2013	*Lab on a chip*
	Quantitative Diagnosis of Malignant Pleural Effusions by Single-Cell Mechanophenotyping[7]	2013	*Science Translational Medicine*
	Real-time deformability cytometry: on-the-fly cell mechanical phenotyping[8]	2015	*Nature Methods*
	Microfluidic cell sorting by stiffness to examine heterogenic responses of cancer cells to chemotherapy[9]	2018	*Cell Death & Disease*
	High-throughput microfluidic compressibility cytometry using multi-tilted-angle surface acoustic wave[10]	2021	*Lab on a chip*
	…… etc[11-13]		
Cell adhesion strength	Probing Cell Adhesion Profiles with a Microscale Adhesive Choice Assay[14]	2017	*Biophysical Journal*
	High-Throughput Characterization of Cell Adhesion Strength Using Long-Channel Constriction-Based Microfluidics[15]	2021	*ACS sensors*
Cell traction force	High-throughput screening for modulators of cellular contractile force[16]	2015	*Integrative Biology*
	Elastomeric sensor surfaces for high-throughput single-cell force cytometry[17]	2018	*Nature Biomedical Engineering*

Supplementary Note. Peeling probe offers significant advantages as a tension sensor compared to TGTs.

Unlike TGTs, the force-induced denaturation of the peeling probe does not result in termination of the mechanical force experienced by adhesion receptors (**Extended Figure 2A**). Note however that TGTs and peeling probes are chemically similar as they are primarily comprised of DNA duplexes. We compared cell spreading area, integrin tension maps (**Extended Figure 2B)**, and the mechanical signaling outcomes for cells incubated on peeling probe or TGT substrates (**Extended Figure 2C**). Quantitative analysis (**Extended Figure 2D**) showed that the spreading area for cells incubated on the peeling probe substrate was significantly larger than that of cells incubated on 12 and 56 pN TGT substrates. The total number of mechanical events was calculated by multiplying the probe density, cell area, and the %peel or %rupture of cells incubated on the three different substrates. There were significantly more total mechanical pulling events for cells incubated on peeling probe substrate versus TGTs, possibly due to two reasons: first, the F_{peel} is ~41 pN, which is less than the T_{tol} for 56 pN TGT; and second, loss of integrin-ligands for TGT substrates modulates cell signaling. Based on the differences in the cell spreading area and tension profile, we sought to further analyze mechanical signaling by quantifying Yes-associated protein (YAP) translocation to the nucleus. YAP translocation to the nucleus is regulated by focal adhesion signaling, F actin organization, and mechanotransduction. YAP nuclear signaling is critical in regulating cell morphology, proliferation, and plasticity.[18] YAP staining showed that cells incubated on peeling probe substrates had the highest YAP nuclear/cyto ratio, followed by 56 pN and then 12 pN TGTs. This result confirms that terminating mechanotransduction through integrin dampens YAP translocation into the cell nucleus, which impairs transcription activation.[19] This result suggests that the peeling probe is better suited to decouple tension sensing from receptor force manipulation within cells in mechanobiology studies, which is highly advantageous.

The oligonucleotides used in this study are listed in **Table S2.**

Table S2. List of oligonucleotides.

construct	oligo	5'	sequence (5' to 3')	3'
TaCT / peeling probe	load-bearing strand	/5ThioMC6-D/	TTT TTT TTT TAG TGA GCT CTG AAG TCT TAG AAC T/iAmMC6T/T TT	/3Bio/
	24mer 5'NH2 peeling strand	/5AmMC6/	AG TTC TAA GAC TTC AGA GCT CAC T	-
	24mer Atto647N and cholesterol peeling strand	/5ATTO647NN/	AG TTC TAA GAC TTC AGA GCT CAC T	/3cholTEG/
	24mer BHQ2 peeling strand	/5BHQ_2/	AG TTC TAA GAC TTC AGA GCT CAC T	-
control duplex	non-fluorescent load-bearing strand	/5ThioMC6-D/	TTT TTT TTT TCA TAC GGT TAT AGA GTA G/iAmMC6T/T TT	/3Bio/
	non-fluorescent peeling strand	/5AmMC6/	CTA CTC TAT AAC CGT ATG	-
TGTs	TGT 12 pN bottom strand	/5AmMC6/	CGC ATC TGT GCG GTA TTT CAC TTT	/3Bio/
	TGT 56 pN bottom strand	/5Biosg/	TT T/iUniAmM/C GCA TCT GTG CGG TAT TTC AC	-
	TGT top quencher strand	/5Hexynyl/	GTG AAA TAC CGC ACA GAT GCG	/3BHQ-2/

The reagents used in this study are listed in **Table S3.**

Table S3. List of reagents.

application	material	company	catalog number
cell culture	Dulbecco's Modified Eagle's Medium (DMEM)	Corning	10-013-cm
	Trypsin	Corning	25-053-CI
	Bovine Calf Serum (CCS)	Corning	35-054-CM
	Fetal Bovine Serum (FBS)	Corning	35-010-CV
	Penicillin-Streptomycin Solution, 100x	Corning	30-002-CI
	Dulbecco's Phosphate-Buffered Saline, 1X without calcium and magnesium	Corning	21-031-CV
cell experiment	Adenosine 5'-diphosphate (ADP)	Sigma	A2754
	UltraPure™ 0.5M EDTA, pH 8.0	Thermo Fisher	15575020
	Latrunculin B	Cayman	10010631
	CellTracker™ Green CMFDA Dye	Thermo Fisher	C7025
oligonucleotide preparation	Atto647N NHS ester	Sigma	18373-1MG-F
	Cy3B NHS ester	GE Healthcare	PA63101
	azide NHS	Thermo Fisher	88902
	Tris(3-hydroxypropyltriazolylmethyl)amine (THPTA)	Sigma	762342
	Nanosep MF centrifugal devices	Pall laboratory	ODM02C35
	P2 gel	Bio-rad	1504118
	Triethylammonium acetate buffer (TEAA)	Sigma	90358
	Bond-Breaker™ TCEP Solution, Neutral pH	Thermo Fisher	77720
	Cyclo[Arg-Gly-Asp-D-Phe-Lys(Mal)]	VIVITIDE	50-168-6952
	Cyclo[Arg-Gly-Asp-D-Phe-Lys(PEG-PEG)]	VIVITIDE	PCI-3696-PI
substrate preparation	(3-Aminopropyl)triethoxysilane	Acros	AC430941000
	Ethanol	Sigma	459836
	Hydrogen peroxide	Sigma	H1009
	EZ-Link™ NHS-Biotin	Thermo Fisher	20217
	Sufuric acid	EMD Millipore	SX1244-6
	Sulfo-NHS acetate	Thermo Fisher	26777
	Wash-N-Dry™ Slide Rack	Sigma	Z758108
	Glass Coverslips for sticky-Slides 25 / 75 mm	Ibidi	10812
	Sticky-slide 18 Well	Ibidi	81818
	ProPlate® 96 Round Well, Bottomless Adhesive Microtiter Plate	Grace bio-labs	204969
	Bovine serum albumin (BSA)	Sigma	735078001
	Dimethyl Sulfoxide (DMSO)	EMD-Millipore	M1096780100
	c(RGDfK(Biotin-PEG-PEG))	VIVITIDE	PCI-3697-PI
	streptavidin	Thermo Fisher	434302
cell fixation and staining	Formaldehyde solution	Sigma	252549
	Triton™ X-100	Sigma	X100
	SiR-Actin Kit	Cytoskeleton	CY-SC001
	Phalloidin-iFluor 647 Reagent	abcam	ab176759
	Recombinant Anti-FAK (phospho Y397) antibody	abcam	ab81298
	Anti-YAP1 Antibody (63.7)	Santa Cruz	sc-101199
	Anti-rabbit IgG (H+L), F(ab')2 Fragment, Alexa488	Cell signaling	4412
	Anti-mouse IgG H&L, Alexa488	abcam	ab150113
	NucBlue™ Fixed Cell ReadyProbes™ Reagent (DAPI)	Thermo Fisher	R37606

The equipment used in this study is listed in **Table S4.**

Table S4. List of equipment.

equipment	company
Barnstead Nanopure water purifying system	Thermo Fisher
Centrifuges	Eppendorf
AdvanceBio Oligonucleotide C18 column, 4.6 x 150 mm, 2.7 µm	Agilent
Grace Alltech C18 column	Grace
High-performance liquid chromatography, 1100	Agilent
Nanodrop 2000 UV-Vis Spectrophotometer	Thermo Fisher
CFI60 Apochromat TIRF 100X Oil Immersion Objective Lens, N.A. 1.49	Nikon
Prime 95B-25mm Back-illuminated sCMOS Camera. 1608x1608,30fps	Photometrics
Nikon Ti2-E Motorized Research Microscope	Nikon
Ti2-ND-P Perfect Focus System 4	Nikon
SOLA SE II 365 Light Engine	Nikon
NIS Elements software	Nikon
C-FL Surface Reflection Interference Contrast (SRIC) Cube, Excitation:535/80nm (495-575nm), Dichroic Mirror: 400nm, No Emission Filter	CHROMA
CF-L AT CY5/Alexa Fluor 647/Draq 5 Filter Set, Excitation: 620/50nm(595-645nm), Emission: 690/50nm (665-715nm), Dichroic Mirror: 655nm	CHROMA
C-FL DS Red Hard Coat, High Signal-to-Noise, Zero Shift Filter Set,Excitation: 545/30nm (530-560nm), Emission: 620/60nm (590-630nm),Dichroic Mirror: 570nm	CHROMA
CF-L AT EGFP/FITC/Cy2/Alexa Fluor 488 Filter Set, Excitation: 480/30nm(465-495nm), Emission: 535/20nm (525-545nm). Dichroic Mirror: 505nm	CHROMA
CytoFLEX V0-B3-R1 Flow Cytometer (equipped with a 488 and a 638 nm laser)	Beckman Coulter

2. Figures

Figure S1. Simulations with oxDNA.

(A) Scheme showing the force-induced peeling mechanism of oligonucleotides. (B) Simulation data of the transition state during force-induced peeling. The transition occurs on µs timescale, which further indicates that the transition state of peeling probe can be ignored while using it as a digital tension sensor. (C) Simulation result of the strand separation distance versus force. (D) Simulated force-distance curve. Conditions used for simulation: loading rate = 2.81×10^3 nm/s, ionic strength = 0.156 M Na^+, and effective stiffness constant k_{eff} = 5.71 pN/nm. The details of the simulation are further described in the methods section.

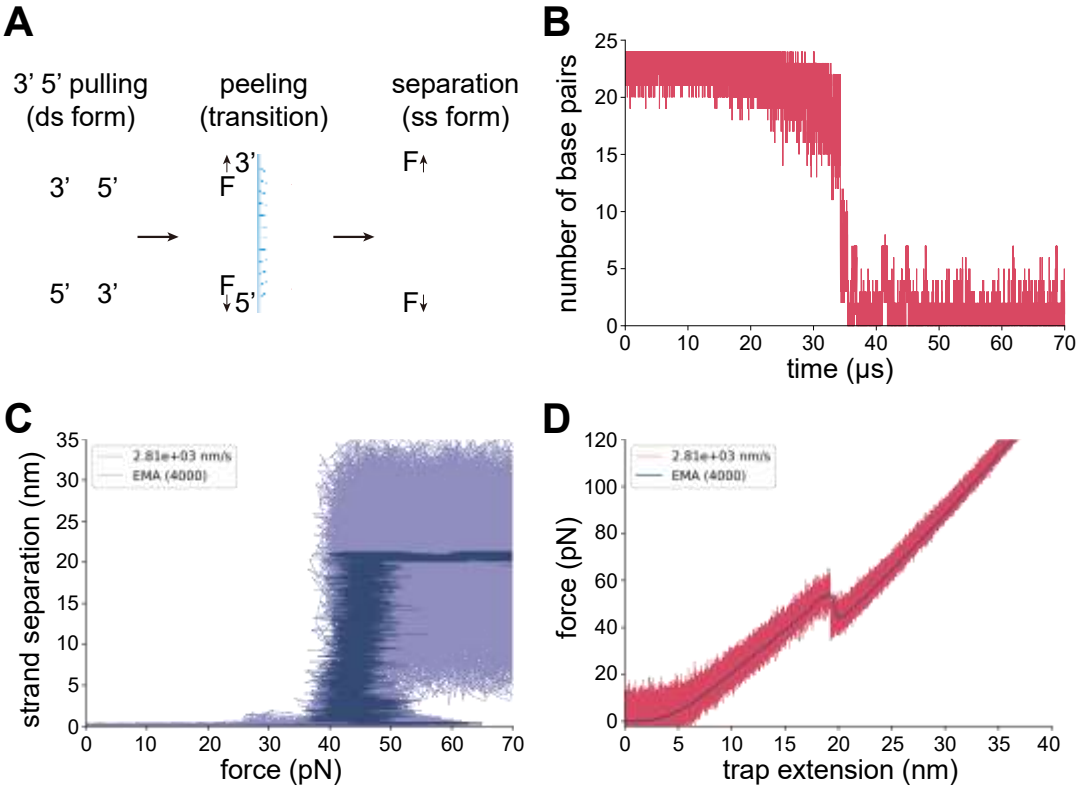

Figure S2. Oligonucleotide preparation.
(A) Chemical structures of the modifications on the oligonucleotides. (B) Schemes showing the modification of DNA strands. (C) HPLC traces showing the purification of the synthesized oligos.

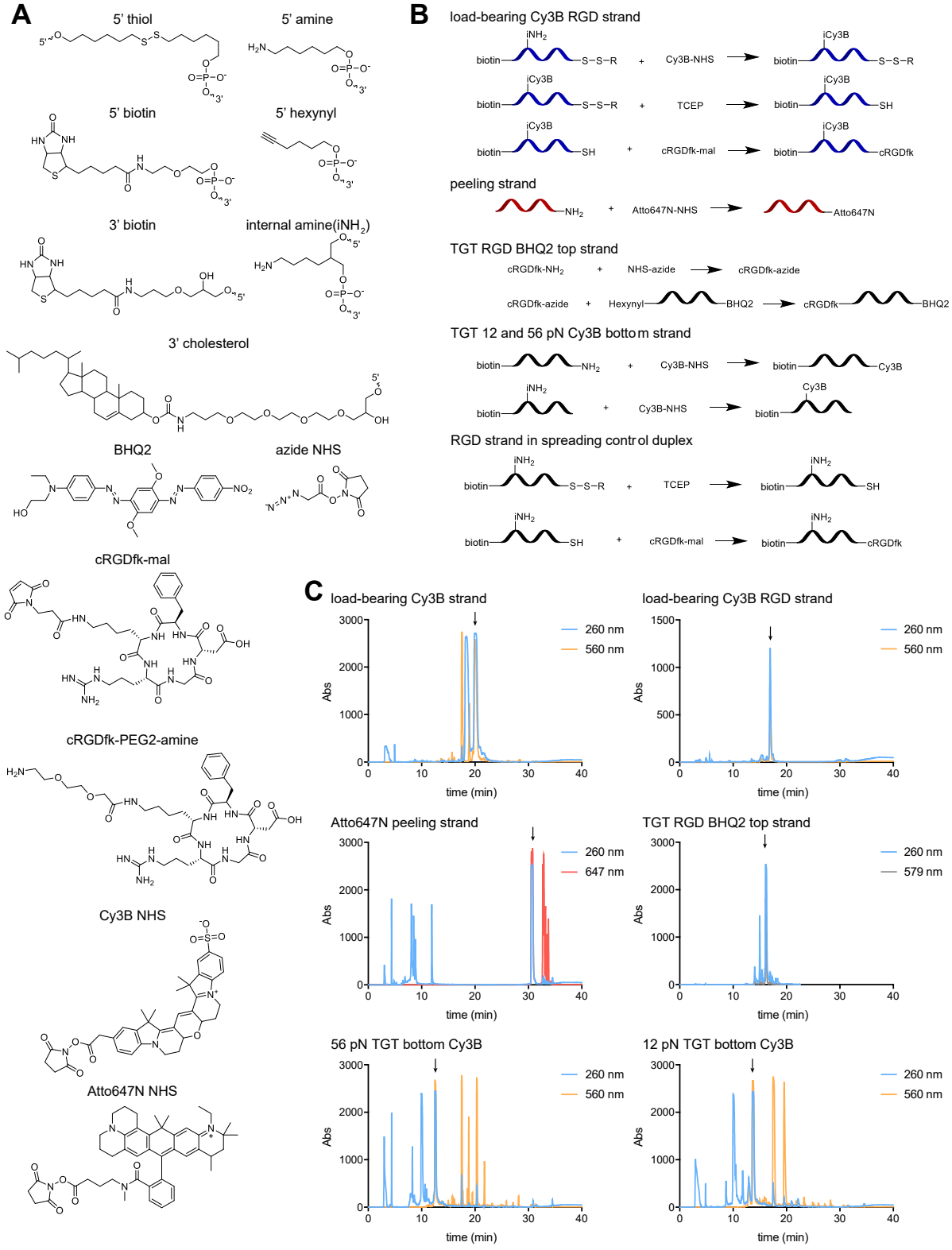

Figure S3. Surface functionalization.
Glass slides were etched in piranha solution and functionalized with 3% APTES. Biotin-NHS was used to react with the amines on the glass slides. After attaching biotinylated glass slide to a sticky slide or a sticky well plate, surfaces were blocked with 1% BSA. Streptavidin was added to bind to the biotin on the surface, and the DNA probes were attached to the surfaces via biotin-streptavidin interaction. After surface preparation, the tension probe substrates were used for tension imaging or TaCT assay.

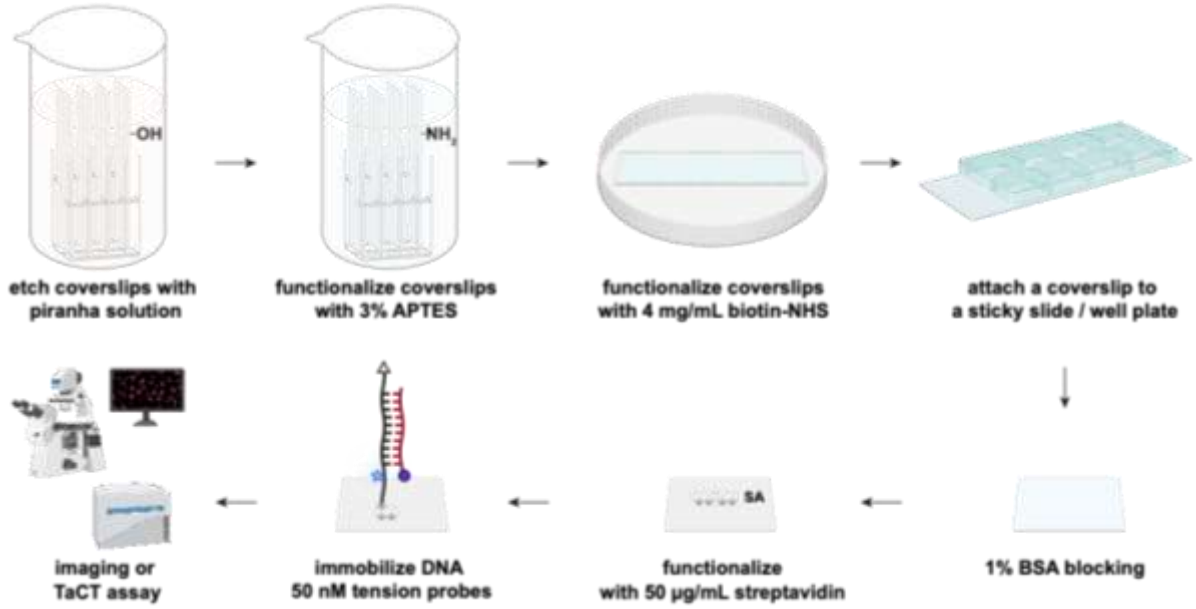

Figure S4. TaCT substrate characterization.
(A) Scheme and representative microscopy images of the TaCT substrate (i) with the acceptor Atto647N (0% peel, I_{DA}), or (ii) without the acceptor Atto647N (mimicking 100% peel, I_D). Scale bar = 20 μm. The Cy3B fluorescence intensity of the substrate (iii) was quantified from multiple XY coordinates from = 3 independent replicates (mean±SD). The FRET efficiency was calculated to be 93.8% using the equation $1 - I_{DA}/I_D$, where I_{DA} is the fluorescence intensity with the donor Cy3B and the acceptor Atto647N present, and I_D is the fluorescence intensity with the donor Cy3B only. (B) The conversion between I_{DA}/I_D and %peel. Briefly, I_{DA}, the fluorescence intensity of the 0% peel substrate (i), and I_D, the fluorescence intensity of 100% peel substrate (ii) were used to generate the conversion function to find the %peel from the fluorescence tension signal. (C) Probe density quantification on TaCT substrates. Lipid standards were prepared by mixing DOPC and TR-DHPE at different percentages, and the fluorescence intensity was measured within the linear range for TR-DHPE in solution and TR-DHPE lipid bilayers on surface to create standard curves. A series of Cy3B-oligo solutions at different concentrations was prepared and their fluorescence intensity in solution was measured to create a standard curve. Data was plotted from 3 replicates (mean±SD). The scaling factor $\boldsymbol{F}_{Cy3B\text{-}TR}$ was calculated using the equation $\boldsymbol{F}_{Cy3B\text{-}TR} = I_{solution(Cy3B\text{-}oligo)}/I_{solution(TR\text{-}DHPE)}$, where I is the concentration normalized fluorescence intensity of the standards (slope).[20] The TR-DHPE molecules per μm^2 was estimated assuming the footprint of a lipid is 0.72 nm^2 and was used for creating the standard curve to find $I_{surface(TR\text{-}DHPE)}$ (note the factor 2 due to the nature of lipid membrane)[21], and the scaling factor $\boldsymbol{F}_{Cy3B\text{-}TR}$ was applied to find the normalized fluorescence intensity $I_{surface(Cy3B\text{-}oligo)}$ of the Cy3B-oligo on surface. The probe density was estimated to be 5242±286 probes/μm^2 from the Cy3B fluorescence intensity of the substrates functionalized with duplexes lacking Atto647N (**Figure S4A, ii**).

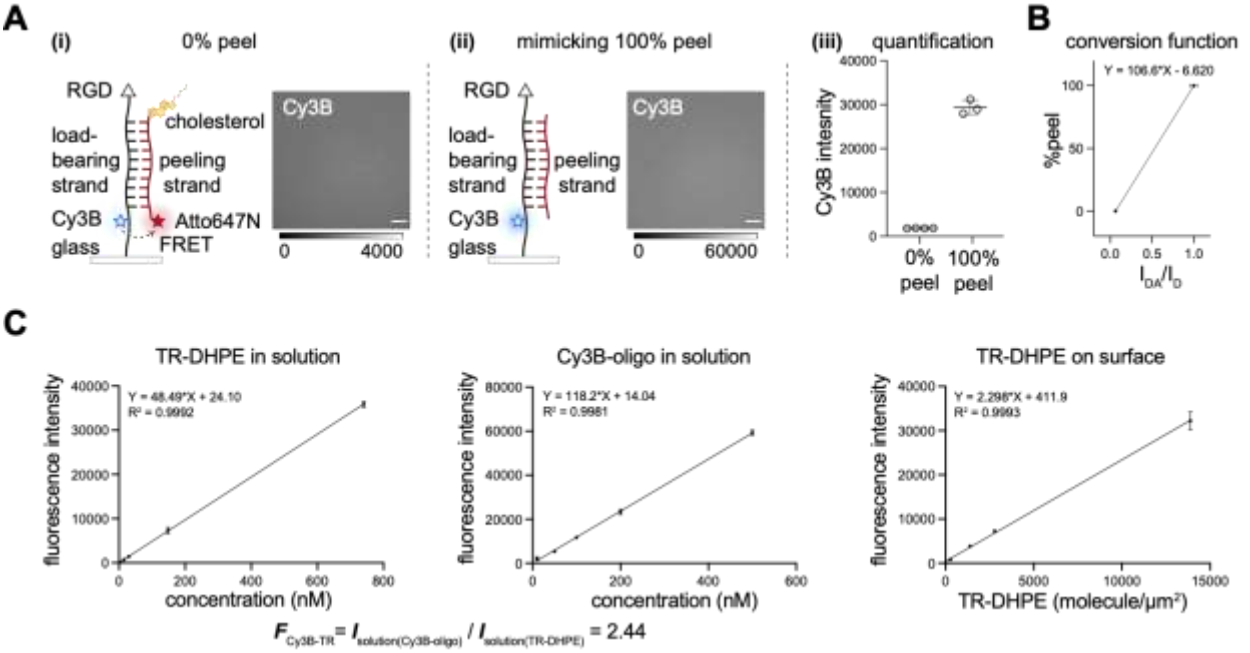

Figure S5. Iterations of DNA probes based on peeling mechanism for microscopy studies on integrin tension.
(A) Scheme shows the tension probe design with only BHQ2 on the peeling strand (n=3). Representative microscopy images in RICM and Cy3B channel show integrin tension produced by MEF cells ~45 min after plating. Scale bar = 10 μm. (B) Scheme shows the tension probe with only Atto647N on the peeling strand (n=3). Representative microscopy images in RICM, Cy3B, and Atto647N channel show integrin tension produced by MEF cells ~45 min after plating. Scale bar = 10 μm. Quenching efficiency and FRET efficiency for iterations in (A) and (B) were calculated using the same method described in **Figure S4** and were used for microscopy data processing. (C) Scheme shows the tension probe with a 18mer duplex region and with only Atto647N on the peeling strand (n=3). Representative microscopy images in RICM, Cy3B, and Atto647N channel show integrin tension produced by mouse platelets ~45 min after seeding. Scale bar = 2 μm. Tension signal was normalized to background fluorescence intensity. We included representative images of the 18mer peeling probe to demonstrate the modularity of the probe. This class of DNA probes is a general design to study molecular tension transmitted through surface receptors. One can change the ligands or change surface chemistry for different cell types to accommodate the need for receptor tension mapping, and presumably one can tune the oligonucleotide to achieve differential F_{peel}.[22]

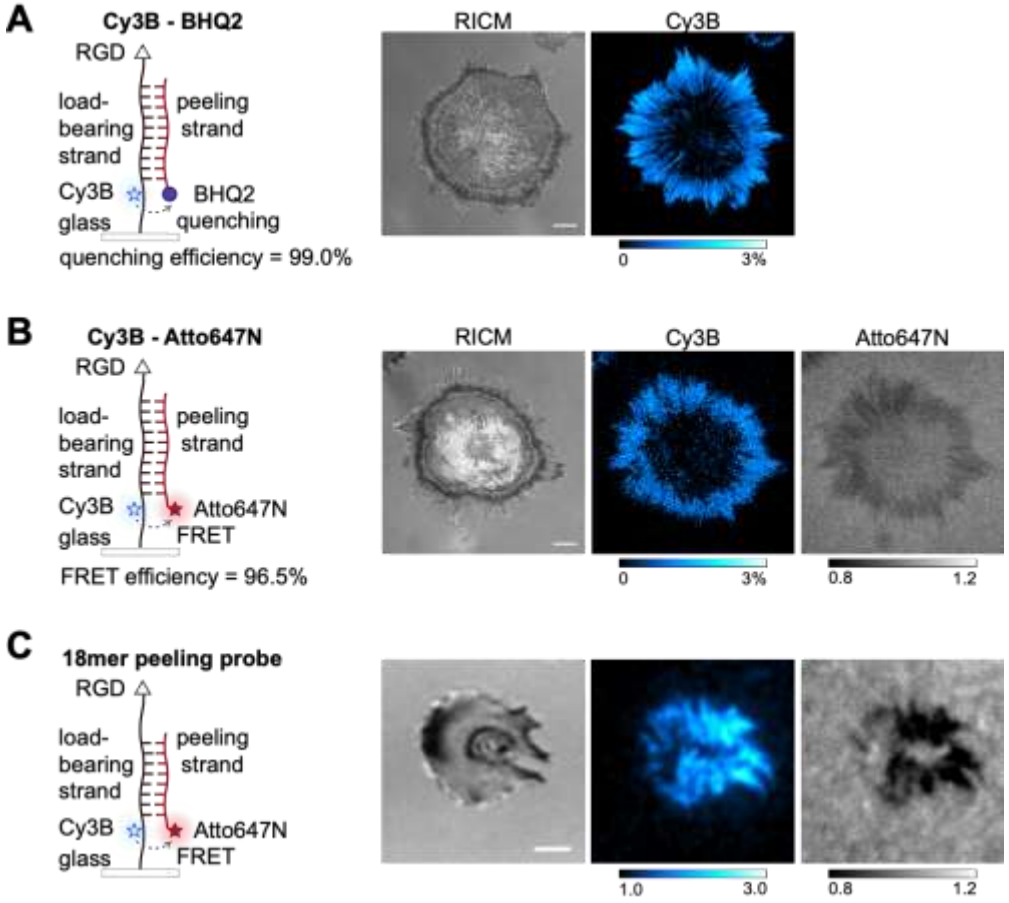

Figure S6. Cholesterol-DNA incorporation in mouse platelets.
Mouse platelets were incubated with 50 nM of different DNA strands and duplexes with or without cholesterol and RGD in Tyrode's buffer at room temperature for 30 min as described in **Extended Figure 4 (see Extended Figure 4A for scheme describing different structures)**. After incubation, platelets were spun down, washed twice, and resuspended in Tyrode's buffer. Samples were divided into 4 portions and the Cy3B and Atto647N fluorescence in cells was measured at t = 0 min, 30 min, 60 min, and 90 min. (A) Representative flow cytometry histogram showing the Cy3B and Atto647N fluorescence in platelets after incubation with DNA strands and duplexes at different time points. (B) Plot showing the Cy3B and Atto647N MFI of platelets incubated with different DNA strands and duplexes from n = 3 experiments, mean±SEM.

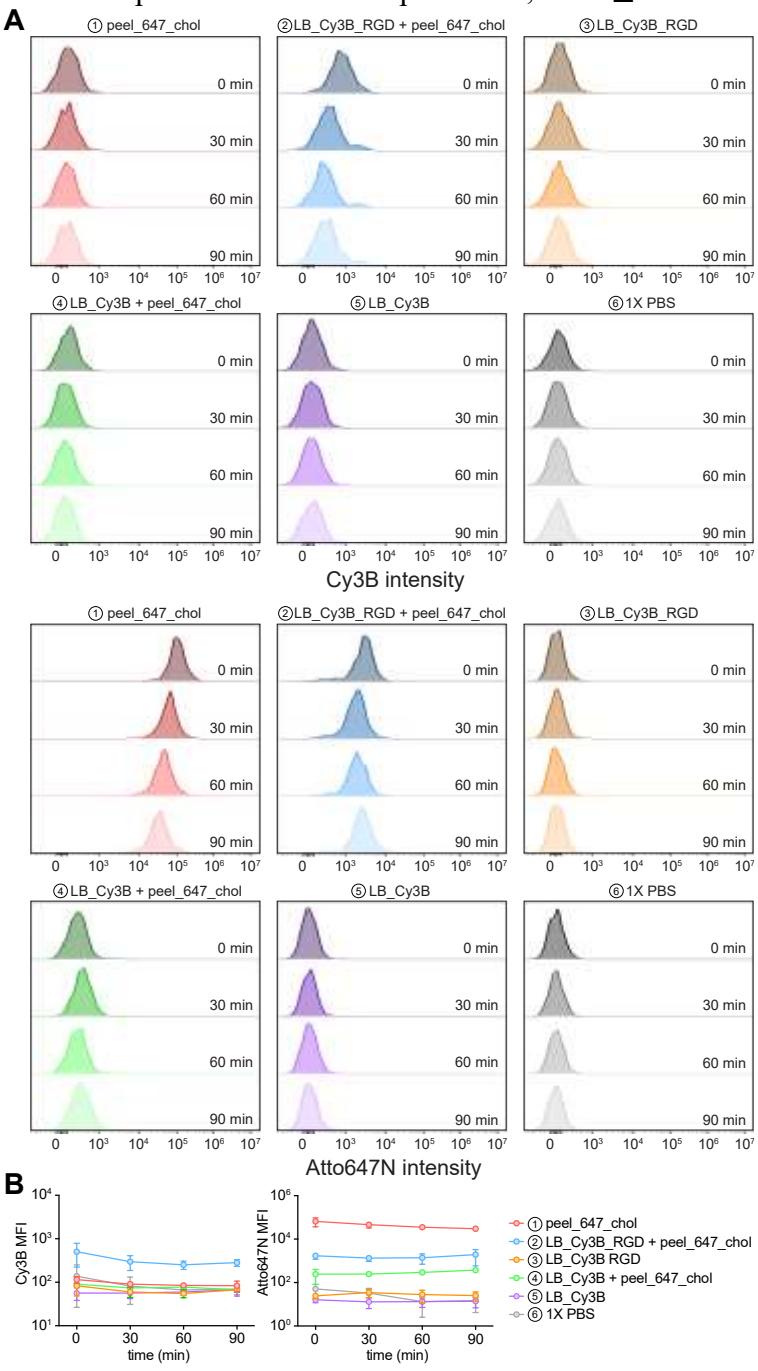

Figure S7. Representative microscopy images of cells pretreated with Y27632.
RICM images show the spreading of the cells pretreated with Y27632 at t = 60 min (n=3). The tension signal in Cy3B channel show the irreversible tension over 60 min after plating the pretreated cells on peeling probe substrates. Scale bar = 10 µm.

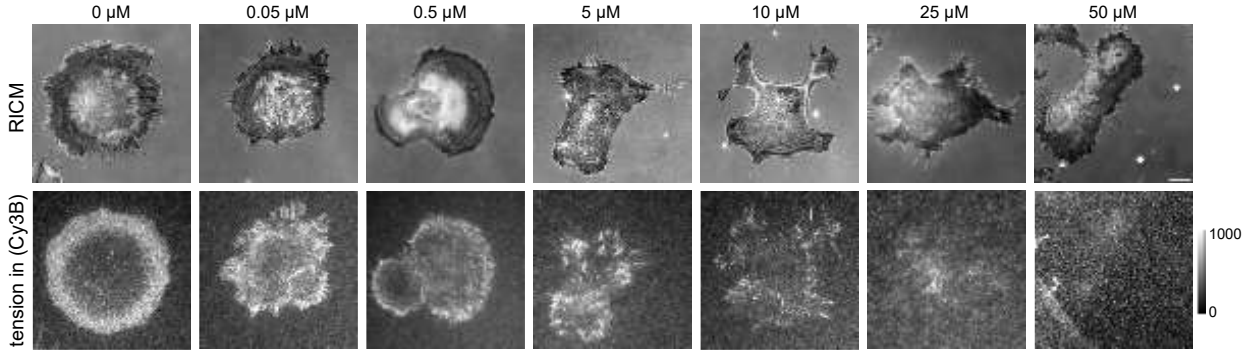

Figure S8. TaCT assay results in MEF WT and MEF vin- cells.
(A) Plot shows the Atto647N gMFI of MEF WT and MEF vin- cells after TaCT when cells were seeded on separate TaCT substrates or mixed and seeded on the same TaCT substrate as described in the maintext and **Figure 2 (**mean ± SEM, paired t-test, two-tailed**)**. The cholesterol-DNA incorporation was measured as a reference for potential differential uptake in WT and vin- cells. WT and vin- cells were incubated with 10 nM Atto647N labeled cholesterol peeling strand in solution in parallel to TaCT assays and the incorporation was measured with the flow cytometer. We chose 10 nM as the cholesterol uptake control, based on microscopy analysis indicating that on average ~46790 ± 2983 peeling strands (7.772×10^{-20} mol) were released per fibroblast. Assuming the height of a spreading cell (mean spreading area = ~1280 µm^2) is ~5 µm, the estimated volume around the cell would be ~6.4×10^{-12} L, and the local concentration of the released cholesterol-DNA would be ~12 nM. (B) Plot shows the Atto647N gMFI values normalized to the cholesterol-DNA uptake. Data acquired from n = 4 replicates, and statistical analysis was performed using two-tailed paired Student t-test.

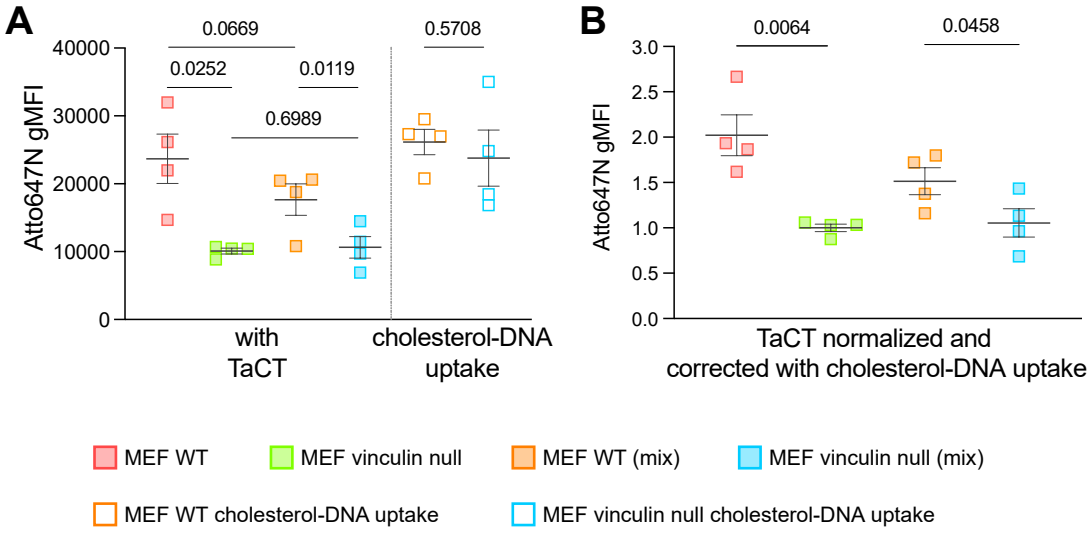

Figure S9. Representative microscopy images of a MEF vin- cell transfected with 3 µg of GFP-vinculin.

Cells were transfected with GFP-vinculin plasmid for 24 h, and then seeded onto TaCT substrates for integrin tension measurements (n=3). Images of cell spreading (RICM), integrin tension (Cy3B), and vinculin expression (vinculin-GFP) were acquired at t=60 min. Scale bar = 10 µm. Scale bar = 10 µm.

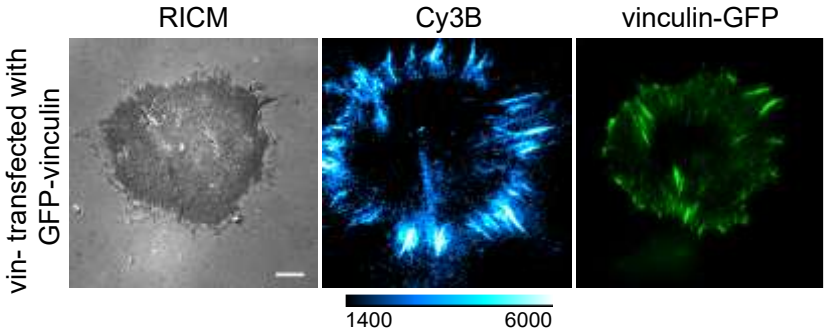

Figure S10. Microscopy data analysis workflow.
Raw fluorescence imaging data was collected and the sCMOS background was subtracted. Three local ROIs were drawn, and the duplex probe background $I_{DA\ resting}$ was measured and averaged. Then, the fluorescence of the fully peeled background I_D was calculated using FRET efficiency calculated from **Figure S4A**. The image was then divided by I_D to obtain an I_{DA}/I_D tension image. The I_{DA}/I_D image was then converted to %peel by applying a predefined conversion function in **Figure S4B, C.**

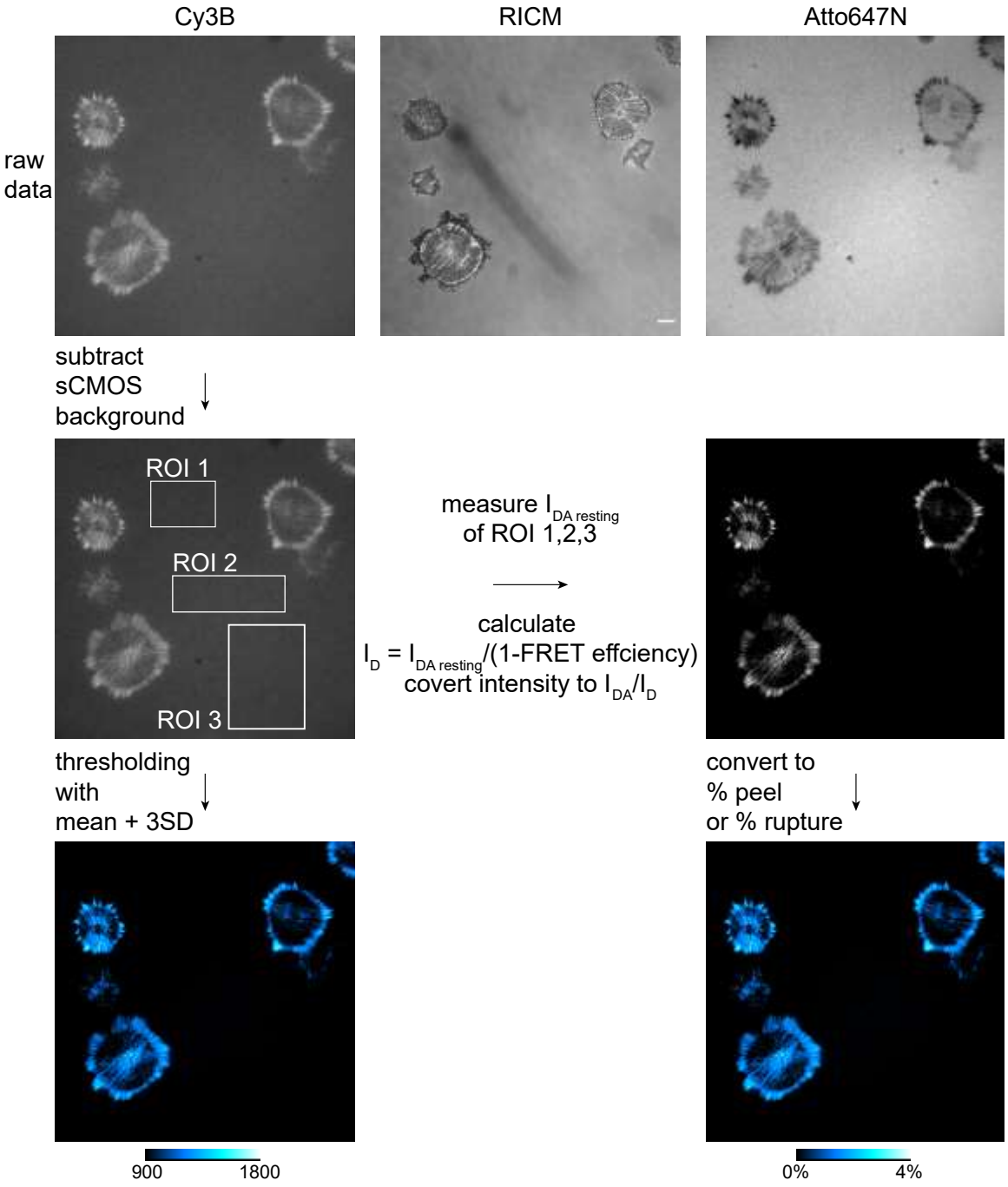

Figure S11. Representative flow cytometry data analysis.
For the flow cytometry analysis of TaCT, viable cells and singlets cells were identified using the forward scatter and side scatter, and the histogram was used to show the fluorescence intensity of viable singlets.

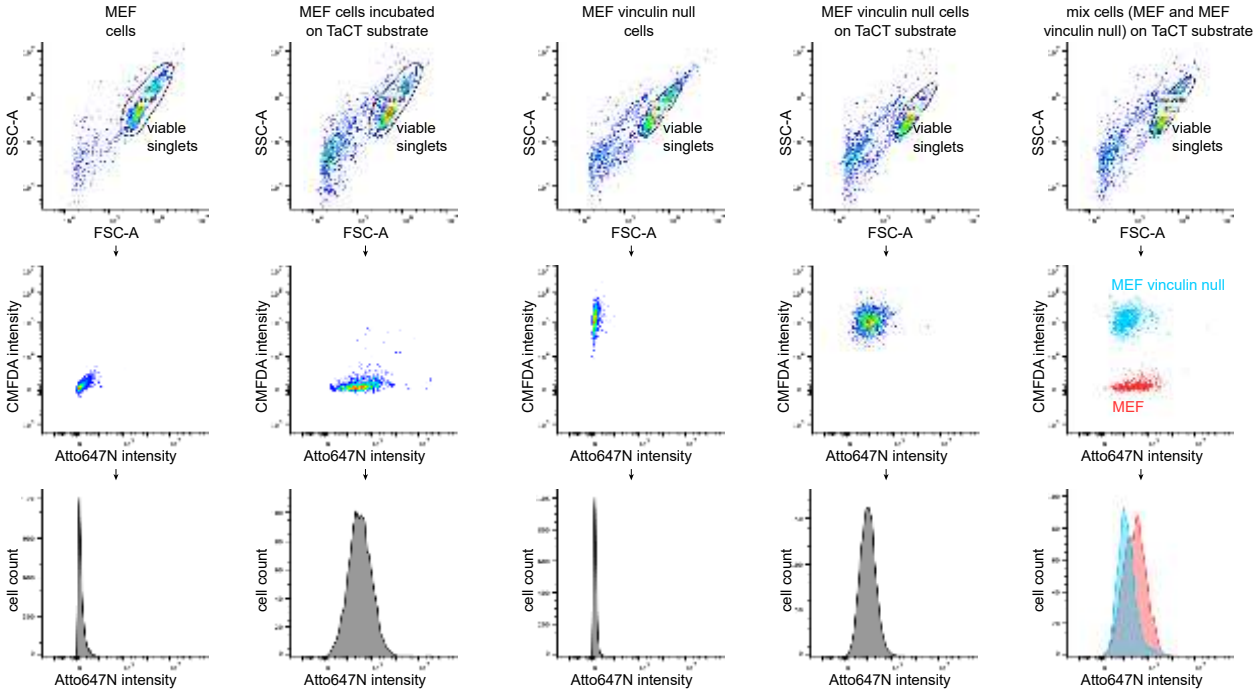

3. Videos

Video S1. Simulation of 24 bp DNA peeling with oxDNA.
Video S2. Fibroblast cell producing integrin tension > 41 pN.

References

1. Guck, J., et al., *Optical deformability as an inherent cell marker for testing malignant transformation and metastatic competence.* Biophys J, 2005. **88**(5): p. 3689-98.
2. Rosenbluth, M.J., W.A. Lam, and D.A. Fletcher, *Analyzing cell mechanics in hematologic diseases with microfluidic biophysical flow cytometry.* Lab Chip, 2008. **8**(7): p. 1062-70.
3. Adamo, A., et al., *Microfluidics-based assessment of cell deformability.* Anal Chem, 2012. **84**(15): p. 6438-43.
4. Guo, Q., S. Park, and H. Ma, *Microfluidic micropipette aspiration for measuring the deformability of single cells.* Lab Chip, 2012. **12**(15): p. 2687-95.
5. Byun, S., et al., *Characterizing deformability and surface friction of cancer cells.* Proc Natl Acad Sci U S A, 2013. **110**(19): p. 7580-5.
6. Dudani, J.S., et al., *Pinched-flow hydrodynamic stretching of single-cells.* Lab Chip, 2013. **13**(18): p. 3728-34.
7. Tse, H.T., et al., *Quantitative diagnosis of malignant pleural effusions by single-cell mechanophenotyping.* Sci Transl Med, 2013. **5**(212): p. 212ra163.
8. Otto, O., et al., *Real-time deformability cytometry: on-the-fly cell mechanical phenotyping.* Nat Methods, 2015. **12**(3): p. 199-202, 4 p following 202.
9. Islam, M., et al., *Microfluidic cell sorting by stiffness to examine heterogenic responses of cancer cells to chemotherapy.* Cell Death Dis, 2018. **9**(2): p. 239.
10. Wu, Y., A.G. Stewart, and P.V.S. Lee, *High-throughput microfluidic compressibility cytometry using multi-tilted-angle surface acoustic wave.* Lab Chip, 2021. **21**(14): p. 2812-2824.
11. Belotti, Y., et al., *High-Throughput, Time-Resolved Mechanical Phenotyping of Prostate Cancer Cells.* Sci Rep, 2019. **9**(1): p. 5742.
12. Kozminsky, M. and L.L. Sohn, *The promise of single-cell mechanophenotyping for clinical applications.* Biomicrofluidics, 2020. **14**(3): p. 031301.
13. Lee, K.C.M., et al., *Toward Deep Biophysical Cytometry: Prospects and Challenges.* Trends Biotechnol, 2021. **39**(12): p. 1249-1262.
14. Kittur, H., et al., *Probing Cell Adhesion Profiles with a Microscale Adhesive Choice Assay.* Biophys J, 2017. **113**(8): p. 1858-1867.
15. Wei, M., et al., *High-Throughput Characterization of Cell Adhesion Strength Using Long-Channel Constriction-Based Microfluidics.* ACS Sens, 2021. **6**(8): p. 2838-2844.
16. Park, C.Y., et al., *High-throughput screening for modulators of cellular contractile force.* Integr Biol (Camb), 2015. **7**(10): p. 1318-24.
17. Pushkarsky, I., et al., *Elastomeric sensor surfaces for high-throughput single-cell force cytometry.* Nat Biomed Eng, 2018. **2**(2): p. 124-137.
18. Dupont, S., et al., *Role of YAP/TAZ in mechanotransduction.* Nature, 2011. **474**(7350): p. 179-83.
19. Cai, X., K.C. Wang, and Z. Meng, *Mechanoregulation of YAP and TAZ in Cellular Homeostasis and Disease Progression.* Front Cell Dev Biol, 2021. **9**: p. 673599.
20. Galush, W.J., J.A. Nye, and J.T. Groves, *Quantitative fluorescence microscopy using supported lipid bilayer standards.* Biophys J, 2008. **95**(5): p. 2512-9.

21. Lin, W.C., et al., *Supported membrane formation, characterization, functionalization, and patterning for application in biological science and technology.* Curr Protoc Chem Biol, 2010. **2**(4): p. 235-69.
22. Yang, Z., et al., *The kinetics of force-dependent hybridization and strand-peeling of short DNA fragments.* Science China Physics, Mechanics & Astronomy, 2016. **59**(8).